Ym1 protein crystals promote type 2 immunity

Ines Heyndrickx[1,2], Kim Deswarte[1,2], Kenneth Verstraete[3,4], Koen H. G. Verschueren[3,4], Ursula Smole[1,2], Helena Aegerter[1,2], Ann Dansercoer[3,4], Hamida Hammad[1,2], Savvas N. Savvides[3,4], Bart N. Lambrecht[1,2,5]

[1]Laboratory of Immunoregulation and Mucosal Immunology, VIB-UGent Center for Inflammation Research, Ghent, Belgium.
[2]Department of Internal Medicine and Pediatrics, Ghent University, Ghent, Belgium.
[3]Unit for Structural Biology, VIB-UGent Center for Inflammation Research, Ghent, Belgium.
[4]Department of Biochemistry and Microbiology, Ghent University, Ghent, Belgium.
[5]Department of Pulmonary Medicine, Erasmus University Medical Center Rotterdam, Rotterdam, The Netherlands.

Abstract

Spontaneous protein crystallization is a rare event, yet protein crystals are frequently found in eosinophil-rich inflammation. In humans, Charcot-Leyden crystals (CLCs) are made from galectin-10 (Gal10) protein, an abundant protein in eosinophils. Whereas mice do not encode Gal10 in their genome, they do form pseudo-CLCs, made from the chitinase-like proteins Ym1 and/or Ym2, encoded by *Chil3* and *Chil4* and made by myeloid and epithelial cells respectively. Here, we investigated the biological effects of pseudo-CLCs since their function is currently unknown. We produced recombinant Ym1 crystals which were shown to have identical crystal packing and structure by X-ray crystallography as *in vivo* native crystals derived from murine lung. When administered to the airways of mice, crystalline but not soluble Ym1 stimulated innate and adaptive immunity and acted as a type 2 immune adjuvant for eosinophilic inflammation via triggering of dendritic cells (DCs). Murine Ym1 protein crystals found at sites of eosinophilic inflammation reinforce type 2 immunity and could serve as a surrogate model for studying the biology of human CLCs.

Corresponding author Bart N. Lambrecht, MD, PhD
Bart.Lambrecht@ugent.be

Keywords: adjuvanticity, protein crystals, Ym1, Ym2, Charcot-Leyden Crystals, Chitinase-like proteins

Introduction

Protein crystals have been described already 150 years ago in eosinophilic inflammatory lesions in humans by Charcot and von Leyden [1-3]. Most proteins can only function properly in the soluble state and spontaneous protein crystallization *in vivo* remains a rare and largely unsolved scientific enigma [4,5].

Protein crystals have also been documented in mouse tissues, almost exclusively in the context of type 2 inflammation, rich in eosinophils, T helper 2 (Th2) cells and alternatively activated macrophages [6-22]. Such crystals in mice are colorless, but in histochemical stains they stain brightly with eosin, consistent with their protein content [14]. Before their biochemical nature was elucidated, they were therefore often referred to as eosinophilic crystals [6]. These murine crystals are frequently observed in aged mice and genetically altered mice on a C57BL/6 or Sv/129 background, and in the context of eosinophil-rich asthma and parasitic infections [6,23]. Although eosinophilic crystals have been documented in the skin, biliary tree, stomach, lymph nodes, spleen and bone marrow of mice, it is clear that the principal site of crystal accumulation is in the lung. In several descriptions, accumulation of eosinophilic crystals was associated with severe lung inflammation and the disease was called eosinophilic crystalline pneumonia, acidophilic macrophage pneumonia or crystalline pneumonitis [7,17,23,24]. In histology slides, the accumulated crystals are variable in size and shape ranging from needle-like crystals to rectangular plates [14]. Their resemblance to the needle-shaped human Charcot-Leyden crystals (CLCs) frequently resulted in the incorrect identification of these murine crystals as CLCs [24,25]. However, only in 2000, almost 100 years after they were first described, Guo *et al*. purified crystals from the bronchoalveolar lavage (BAL) fluid of viable motheaten (me^v/me^v) mice and mass spectrometry analysis identified the chitinase-like protein (CLP) Ym1 as the sole protein component [6], thereby providing an unambiguous annotation of their content and distinguishing them from CLCs. Human CLCs are comprised of the eosinophil-derived galectin-10 (Gal10) protein, which is not encoded in the mouse genome [26,27]. Ym1 is mainly produced by alveolar macrophages, alternatively activated "M2" macrophages, neutrophils and a subset of circulating pro-repair monocytes [28-30]. In hyaline gastric lesions of aged 129S4/SvJae and B6,129 CYP1A2 null mice, pseudo-CLCs were found to consist of the closely related CLP Ym2, which is a protein mainly made by epithelial cells under the influence of IL-13 [14,25,31,32]. Ym1 (encoded by the *Chil3* gene) and Ym2 (encoded by the *Chil4* gene) are CLPs belonging to the glycoside hydrolase family 18 (GH18) and are unique to mice, with no known human orthologues [33]. Their potential receptors and natural binding partners are largely unknown, as are the exact functions of these still very enigmatic proteins. We previously reported that recombinant Gal10 crystals produced *in vitro* showed crystal packing and structure identical to CLCs derived from patient mucus. When administered to the airways of mice, Gal10 crystals stimulated innate and adaptive immunity and acted as a type 2 adjuvant [34]. Since mice do not encode the *LGALS10* gene, Gal10 has the potential to act as a neo-antigen in this setting. Here, we tested the *in vivo* relevance of pseudo-CLCs since these are made endogenously in mice at sites of eosinophilic inflammation, albeit mainly by macrophages and epithelial cells. We showed that recombinant *in vitro* made Ym1 and Ym2

crystals were structurally similar to crystals isolated from mice and to each other, and when administered to the airways of mice, crystalline Ym1, but not soluble Ym1 protein stimulated innate and adaptive immunity and acted as an adjuvant for Th2 driven eosinophilic airway inflammation and immunoglobulin secretion.

Materials and methods

Mice

Female wild type (WT) C57BL/6 mice were purchased from Janvier Labs (Saint-Berthevin, France), housed under specific pathogen-free conditions and used between 6 and 8 weeks of age. Investigators were not blinded to group allocation during experiments. No animals were excluded from the analysis. All experiments were approved by the animal ethics committee at Ghent University and were in accordance with Belgian animal protection law.

Production of recombinant Ym1 and Ym2 protein and crystals

A synthetic codon-optimized DNA sequence (Genscript) encoding murine Ym1 (Uniprot ID O35744, residues 22 – 398) was cloned in the pCAGG mammalian expression vector in frame with the mouse IgH signal peptide (MGWSCIIFFLVATATGVHS). A synthetic codon-optimized DNA sequence (Genscript) encoding murine Ym2 (Uniprot Q91Z98, residues 22 - 402) was cloned in the pTwist-CMV-BetaGlobin mammalian expression vector (Twist Biosciences) in frame with the mouse IgH signal peptide (MGWSCIIFFLVATATGVHS), and an N-terminal hexahistine-tag followed by a Tobacco Etch Virus (TEV)-protease cleavage site.

Ym1 and Ym2 were produced in FreeStyle 293-F cells in suspension. Cells were transfected with 1 μg/ml DNA using 2-fold excess of linear polyethylenimine (PEI; Polysciences). Conditioned medium containing the secreted recombinant protein was collected 4 days post transfection and filtered. Medium containing Ym1 was dialyzed to 20 mM Tris pH 8.0 and the Ym1 protein was purified via Q Sepharose anion exchange chromatography. Ym1 was further purified to a pure solution via size-exclusion chromatography using phosphate-buffered saline (PBS) as running buffer. Ym2 was purified from the clarified conditioned medium via immobilized metal affinity chromatography (IMAC) and size-exclusion chromatography with PBS buffer. Endotoxin levels were determined with an Endosafe-PTS system (Charles River) to be lower than 1 EU/mg of recombinant protein. To form recombinant Ym1 crystals, recombinant Ym1 protein (3 to 4 mg/ml) was incubated with 1M Na-acetate buffer pH 4.6 with a buffer:target protein ratio of 1:10 (v/v). During a 24h incubation the protein solution was agitated a few times by inverting it five times, after which the solution turned cloudy due to the formation of protein crystals. The crystal-containing suspension was spun down (400g for 5 min) and washed three times with sterile and endotoxin-free PBS before the crystals were resuspended in 1 ml of sterile and endotoxin-free PBS. The total protein concentration of this solution was determined by solubilizing 20 µl of the crystal suspension in an equal volume of 6M guanidinium hydrochloride and measuring the absorbance at 280 nm with a Thermo Scientific NanoDrop 2000. The calculated extinction coefficient for Ym1 was 77155 $M^{-1}\,cm^{-1}$.

117

118 **Crystallographic structure determination of *ex vivo* and recombinant Ym1 and Ym2 crystals**

119 Single *ex vivo* Ym1 and Ym2 crystals were harvested from the BAL fluid of me^v/me^v mice and
120 C57BL/6J-Tg(CAG-Gal10)^{Bla} mice by using mounted cryo-loops. Before being cryo-cooled in
121 liquid nitrogen, crystals were cryo-protected by a brief soak in PBS supplemented with 35%
122 (v/v) ethylene glycol (Ym1) or 35 % glycerol (Ym2). Recombinant Ym1 was crystallized in
123 condition A7 of the Hampton Research Crystal Screen HT (0.1 M sodium cacodylate pH 6.5,
124 1.4 M sodium acetate) via vapor diffusion sitting drop crystallization experiments, and crystals
125 were cryo-protected with mother liquor supplemented with 30% (v/v) glycerol. Following
126 overnight incubation with TEV-protease, recombinant Ym2 was crystallized via vapor diffusion
127 sitting drop crystallization experiments using 0.1 M sodium acetate pH 6.0 and 200 mM $CaCl_2$
128 as mother liquor, and crystals were cryoprotected with 30% (v/v) PEG-400. Diffraction
129 experiments at 100 K were conducted on beamlines Proxima 1 (SOLEIL synchrotron, Saint-
130 Aubin, France), P14 of Petra III (DESY, Hamburg, Germany) and X06SA (PXI) of the Swiss Light
131 Source (Paul Scherrer Institute, Villigen, Switzerland). All data were integrated and scaled
132 using the XDS suite[35] and the CCP4 suite [36]. Molecular replacement was executed using Phaser
133 [37] employing the structure of Ym1 (pdb: 1vfb) as a search model. Further rebuilding of the
134 model and refinement was performed in *COOT* [38] and autoBuster [39]. Map and model validation
135 was monitored throughout the refinement procedure using *COOT*, the CCP4 package and
136 PDB_REDO server [40].

137

138 ***In vivo* models**

139 To analyze the innate immune responses, WT C57BL/6 mice were injected intratracheally (i.t.)
140 with 100 µg Ym1 crystals or 100 µg soluble Ym1 diluted in 80 µl of PBS. After 6 and 24 hours,
141 mice were euthanized by CO_2 inhalation or an overdose of pentobarbital (KELA Laboratoria)
142 and BAL fluid and lungs were collected.

143 To analyze dendritic cell (DC) activation, WT C57BL/6 mice were injected i.t. with 5 µg Alexa
144 Fluor 488-labeled ovalbumin (OVA-AF488) mixed with 100 µg Ym1 crystals or with 100 µg
145 soluble Ym1 diluted in 80 µl of PBS. After 24 hours, mice were euthanized by CO_2 inhalation
146 and mediastinal lymph nodes (mLNs) were collected.

147 To analyze the adaptive cellular immune responses, CD4+ OT-II KN2 cells were purified from
148 CD45.1.2 OT-II KN2 donor mice with the MojoSort™ Mouse CD4 T Cell Isolation Kit (Biolegend)
149 and labeled with cell proliferation dye eFluor 450 (0.01 mM; Thermo Fisher Scientific) for 10
150 min in the dark at 37°C. Next, 1×10^6 of these labeled cells (in 100 µl of PBS) were injected
151 intravenously (i.v.) into WT C57BL/6 mice and subsequently, mice were injected i.t. with 10 µg
152 ovalbumin (OVA, Worthington) or with 10 µg OVA mixed with 100 µg of Ym1 crystals or 100
153 µg soluble Ym1 (in 80 µl of PBS). For this experiment, OVA was pre-filtered through a 0.22 µm
154 filter. On day 4 and 7, mice were euthanized by CO_2 inhalation and mLNs and lungs were
155 collected.

156 To analyze the adaptive humoral immune responses, WT C57BL/6 mice were injected
157 intraperitoneally (i.p.) on day 0 with 0.5 mg Ym1 crystals or 0.5 mg soluble Ym1, on day 7 with

158 0.5 mg Ym1 crystals and on day 14 with 0.5 mg Ym1 crystals or 10 µg Sol Ym1 all diluted in 500
159 µl PBS. On day 21 mice were euthanized with an overdose of pentobarbital (KELA Laboratoria)
160 and blood was collected.
161 To analyze the type 2 adjuvanticity of Ym1 crystals, WT C57BL/6 mice were sensitized i.t. on
162 day 0 and day 1 with 100 µg OVA (Worthington), 100 µg OVA mixed with 100 µg of Ym1 crystals
163 or 100 µg OVA mixed with 100 µg soluble Ym1 diluted in 80 µl PBS. On days 11 to 13, all mice
164 were challenged daily intranasally (i.n.) with 20 µg of OVA (Worthington) diluted in 40 µl of
165 PBS. One day after the last challenge, on day 14, mice were euthanized with an overdose of
166 pentobarbital (KELA Laboratoria) and blood, BAL fluid and mLNs were collected.
167 All i.t. and i.n. treatments were given after mice were anesthetized with isoflurane (2
168 liters/min, 2 to 3%; Abbott Laboratories).
169 Blood was obtained from the iliac vein and centrifuged at 10000 rpm for 10 min at room
170 temperature (RT). Serum was collected and stored at −20 °C until further use (serum antibody
171 ELISA). BAL was performed by injecting PBS containing 0.01 mM EDTA (Lonza) through a
172 tracheal canula. Subsequently, BAL fluid was centrifuged (400g for 5 min at 4°C). The
173 supernatant was collected and stored at −20°C until further use (cytokine ELISA) and the pellet
174 was used for ImageStream or flow cytometry. To obtain lung and mLN single-cell suspensions
175 for flow cytometry, lungs and mLNs were first cut with a scissor and then digested at 37°C for
176 30 or 15 min respectively in RPMI-1640 (ThermoFisher Scientific) containing Liberase TM (20
177 µg/ml; Merck) and deoxyribonuclease (DNase) I (0.01 U/µl; Merck). The resultant cell
178 suspensions were filtered through a 70 µm filter. To obtain mLN single-cell suspensions for
179 flow cytometry or mLN restimulation cultures, mLNs were smashed on a 70 µm filter. To
180 measure pro-inflammatory cytokines, lungs were snap frozen in liquid nitrogen and
181 homogenized with a TissueLyser II from Qiagen in tissue lysis buffer [40 mM tris-HCL (pH 6.8),
182 275mM NaCl and 20% glycerol (Sigma-Aldrich)]. One tablet of PhosSTOP (Sigma-Aldrich) and
183 one tablet of Complete ULTRA tablets, Mini, Easypack (Sigma-Aldrich) were added per 10 ml
184 of tissue lysis buffer. After homogenization, 2% IGEPAL CA-630 (U.S. Biological) was added.
185 Subsequently, the samples were rotated for 30 min and centrifuged (20000g for 10 min at
186 4°C). Supernatants were stored at −20°C. The total protein concentration was measured with
187 the NanoOrange protein quantitation kit from Thermo Fisher Scientific.
188
189 **Flow cytometry**
190 Prior to staining for flow cytometry, single-cell suspensions were depleted of red blood cells
191 (RBCs) by using RBC lysis buffer [0.15 M NH4Cl (Merck), 1 mM KHCO3 (Merck), and 0.1 mM
192 Na2-EDTA (Merck) in MilliQ H2O] produced in-house. For all flow experiments, single cell
193 suspensions were incubated with the eBioscience™ Fixable Viability Dye eFluor™ 506
194 (ThermoFisher Scientific) to identify dead cells. Fc Block 2.4.G2 (Bioceros) was used to block
195 aspecific antibody binding. Cell surface markers were stained for 30 min at 4°C in the dark.
196 123count eBeads™ Counting Beads (ThermoFisher Scientific) were added to each sample to
197 determine absolute cell numbers. Settings were calibrated using UltraComp eBead™

198 Compensation Beads (ThermoFisher Scientific). Data were acquired on an LSR Fortessa with
199 FACS Diva software (BD Biosciences) and were analyzed with FlowJo software (Tree Star).
200 For the analysis of innate immune responses, lung single-cell suspensions were stained for
201 flow cytometry using FITC-conjugated anti-Ly-6C (AL-21) (BD Biosciences), PE-conjugated anti-
202 Siglec-F (E50-2440) (BD Biosciences), PE-Cy5-conjugated anti-CD3e (145-2c11) (Thermo Fisher
203 Scientific), PE-Cy5-conjugated anti-CD19 (1D3) (Thermo Fisher Scientific), PE-Cy7-conjugated
204 anti-CD11c (N418) (Thermo Fisher Scientific), BD Horizon V450-conjugated anti-CD11b
205 (M1/70) (BD Biosciences), Brilliant Violet 605-conjugated anti-CD45 (30-F11) (BD Biosciences),
206 Alexa Fluor 647-conjugated anti-CD64 (X54-5/7.1) (BD Biosciences), Alexa Fluor 700–
207 conjugated anti-Ly6G (1A8) (BD Biosciences) and APC-eFluor 780–conjugated anti-I-A/I-E
208 (M5/114.15.2) (Thermo Fisher Scientific).
209 For the analysis of DC activation, mLN single-cell suspensions were stained for flow cytometry
210 using PerCP-Cy5.5-conjugated anti-CD80 (16-10A1) (BioLegend), eFluor 450-conjugated anti-
211 CD11c (N418) (ThermoFisher Scientific), Brilliant Violet 650-conjugated anti-XCR1 (ZET)
212 (BioLegend), Brilliant Violet 711-conjugated anti-CD64 (X54-5/7.1) (BioLegend), Alexa Fluor
213 647-conjugated anti-CD172a (P84) (BioLegend), Alexa Fluor 700- conjugated anti-Ly-6C (AL-
214 21) (BD Biosciences), APC-eFluor 780-conjugated anti-MHCII (M5/114.15.2) (ThermoFisher
215 Scientific), PE-conjugated anti-CD88 (20/70) (BioLegend), biotin-conjugated anti-CCR7 (4B12)
216 (ThermoFisher Scientific) + PE-CF594-conjugated streptavidin (BD Biosciences), PE-Cy5-
217 conjugated anti-CD3e (145-2c11) (ThermoFisher Scientific), PE-Cy5-conjugated anti-CD19
218 (1D3) (Thermo Fisher Scientific), PE-Cy7-conjugated anti-CD86 (PO3) (BioLegend), BUV395-
219 conjugated anti-CD11b (M1/70) (BD Biosciences) and BUV737-conjugated anti-CD26 (H194-
220 112) (BD Biosciences).
221 For T cell response analysis, mLN and lung single-cell suspensions were stained using
222 FITC-conjugated anti-Va2 TCR (B20.1) (BD Biosciences), Brilliant Violet 605-conjugated anti-
223 CD45.1 (A20) (BioLegend), RedFluor710-conjugated anti-CD44 (IM7) (Thermo Fisher
224 Scientific), APC-eFluor780-conjugated anti-CD25 (PC61.5) (Thermo Fisher Scientific), PE-
225 conjugated anti-CD62L (MEL-14) (BD Biosciences), biotin-conjugated anti-hCD2 (RPA-2.10)
226 (BioLegend) + PE-CF594-conjugated streptavidin (BD Biosciences), PE-Cy7-conjugated CD3e
227 (145-2C11) (BioLegend), BUV395-conjugated anti-CD4 (GK1.5) (BD Biosciences) and BUV737-
228 conjugated anti-CD45.2 (104) (BD Biosciences).
229 BAL cells were stained with PE-conjugated anti-Siglec F (E50-2440) (BD Biosciences), PE-Cy5-
230 conjugated anti-CD3e (145-2c11) (ThermoFisher Scientific), PE-Cy5-conjugated anti-CD19
231 (1D3) (Thermo Fisher Scientific), PE-Cy7-conjugated anti-CD11c (N418) (ThermoFisher
232 Scientific), BD Horizon V450-conjugated anti-CD11b (M1/70) (BD Biosciences), Alexa Fluor
233 700-conjugated anti-Ly6G (1A8) (BD Biosciences) and APC-eFluor 780-conjugated anti-MHCII
234 (M5/114.15.2) (Thermo Fisher Scientific).
235
236 **ImageStream**
237 For ImageStream analysis, the pellets obtained after centrifugation of the BAL fluid were
238 pooled and stained for 30 min at 4°C with unconjugated polyclonal goat anti-mouse Ym1/2

239 (AF2446, R&D Systems; 1:100 diluted in PBS). After washing, the pellet was stained for 30 min
240 at 4°C in the dark with Alexa Fluor 647-conjugated polyclonal donkey anti-goat IgG
241 (ThermoFisher Scientific; 1:1000 diluted in PBS). Fc Block 2.4.G2 (Bioceros) was used to block
242 aspecific antibody binding. Data were acquired on an Amnis ImageStreamX Mk II with
243 INSPIRE™ software (Luminex) and were analyzed with IDEAS® software (Luminex).
244
245 **Enzyme-linked immunosorbent assay (ELISA)**
246 Interleukin (IL)-1β, IL-5, IL-6, IL-10, IL-13, IL-33, tumor necrosis factor alpha (TNFα) and C-C
247 motif chemokine ligand 2 (CCL2) concentrations were evaluated using the Ready-SET-Go!™
248 ELISA kits (ThermoFisher Scientific). CCL24 concentrations were evaluated using the Mouse
249 CCL24/Eotaxin-2/MPIF-2 DuoSet ELISA kit (R&D Systems). Serum Ym1-specific
250 immunoglobulin M (IgM) and OVA-specific immunoglobulin G1 (IgG1) antibody levels were
251 determined in flat-bottom 96-well plates (Greiner Bio-One), coated overnight with 0.1 mg/ml
252 soluble Ym1 in PBS or with 0.1 mg/ml OVA (Worthington) in 0.1 M sodium carbonate buffer
253 (pH 9.5), respectively. After washing and blocking for 1 hour, the samples diluted in PBS were
254 added in duplicate and incubated for 2.5 hours at RT. After washing, biotinylated anti-mouse
255 IgG1 or IgM detecting antibody (0.5 mg/ml; BD Biosciences) plus streptavidin-HRP reagent
256 (1:250; BD Biosciences) was added and incubated for 1 hour at RT. After another wash step,
257 1× TMB substrate solution (Thermo Fisher Scientific) was added and to stop the reaction, 2.5N
258 H_2SO_4 was used. Finally, the absorbance was read at 450 nm (and 650 nm as reference) with
259 a Perkin Elmer multilabel counter and data were collected with Wallac 1420 Manager software
260 (PerkinElmer).
261
262 **Statistical analysis**
263 Experiments shown in Figure 2 were analyzed with an ordinary two-way ANOVA test with
264 Tukey's multiple comparisons test. For all experiments in Figure 3, 4 and 5, the normality of
265 each group was first checked by using the Shapiro-Wilk statistical test. Parametric data were
266 analyzed with an ordinary one-way ANOVA test with Šidák's multiple comparison correction
267 and nonparametric data were analyzed with a Kruskal-Wallis test with Dunn's multiple
268 comparison correction. All statistical tests were performed in GraphPad Prism software
269 (GraphPad Software).
270
271 **Supplementary Online Material**
272 This paper has an online data supplement. Table S1 describes the key crystallographic data of
273 *ex vivo* isolated Ym1 and Ym2 crystals for comparison with *in vitro* generated recombinant
274 Ym1 and Ym2 crystals.
275
276 **Results**
277 **Recombinant Ym1 and Ym2 crystals are structurally similar to native crystals *ex vivo*.**
278 Individual crystals were harvested from the BAL fluid of me^v/me^v mice (carrying a defective
279 protein tyrosine phosphatase SHP-1 gene) developing crystalline pneumonia [6] and C57BL/6J-

280 Tg(CAG-Gal10)^{Bla} mice (transgenically overexpressing Gal10 from the ubiquitous CAG
281 promotor, manuscript in preparation), sensitized and challenged with the allergen house dust
282 mite (HDM). Crystallographic studies using microfocus synchrotron X-rays showed that the
283 crystals obtained from the BAL fluid of me^{v}/me^{v} mice were Ym1 crystals, in accordance with a
284 previous report [6]. We had hypothesized that the crystals obtained from the BAL fluid of
285 C57BL/6J-Tg(CAG-Gal10)^{Bla} mice were CLCs containing Gal10. However, crystallographic
286 characterization of these crystals revealed that they are Ym2 crystals. In parallel, we produced
287 recombinant Ym1 and Ym2 protein in FreeStyle 293-F cells. Spontaneous crystallization was
288 aided by low pH and low temperature (4°C) (Fig. 1 A, B). Native *in vivo* isolated Ym1 crystals
289 and recombinant Ym1 crystals (Fig. 1 C) as well as native *in vivo* isolated Ym2 crystals and
290 recombinant Ym2 crystals (Fig. 1 D) were crystallographically equivalent, sharing the same
291 monoclinic space group (P21) and unit-cell parameters. Moreover, X-ray crystallographic
292 studies showed that a native *in vivo* isolated Ym1 crystal and a native *in vivo* isolated Ym2
293 crystal are structurally similar to each other, which is not so surprisingly as Ym1 (*Chil3*) and
294 Ym2 (*Chil4*) are two closely related proteins sharing 95% nucleotide sequence identity and
295 91% amino acid sequence identity (Fig. 1 E, F, G). Crystallographic data and refinement
296 statistics can be found in Table S1. Thus, recombinant Ym1 and Ym2 protein crystals can be
297 generated *in vitro* and are biosimilar to native Ym1 and Ym2 crystals.
298
299 **Ym1 crystals activate innate immunity.**
300 We next addressed whether Ym1 crystals could have pro-inflammatory effects in the lungs.
301 Naïve WT C57BL/6 mice received an i.t. injection of 100 µg of endotoxin-low Ym1 crystals or
302 control soluble Ym1 (Fig. 2 A). After 6 and 24 hours, there was a prominent influx of Ly6C^{+}
303 monocytes and eosinophils into the airways of mice receiving Ym1 crystals but not in those
304 receiving soluble Ym1 or PBS. Neutrophil numbers were also increased in the Ym1 crystal
305 group, but this failed to reach statistical significance (Fig. 2 B). This influx was accompanied by
306 the production of the innate pro-inflammatory cytokines IL-6 and TNFα in BAL fluid (Fig. 2 C)
307 and the inflammasome-dependent cytokine IL-1β and the alarmin IL-33 in lung tissue only in
308 the group receiving crystalline Ym1 (Fig. 2D). Other cytokines like IL-1α and granulocyte-
309 macrophage colony-stimulating factor (GM-CSF) were not consistently induced in any of the
310 groups (data not shown). The monocyte chemoattractant CCL2 and the eosinophil
311 chemoattractant CCL24 (Eotaxin-2) were found enhanced in lung tissue of the crystal-treated
312 group (Fig. 2 E), particularly at early time points, suggesting these paracrine signals were
313 driving the cellular influx induced by crystals.
314 As we were unable to make a crystallization-deficient soluble Ym1 mutein, we used WT soluble
315 Ym1 protein as a control. However, we took into consideration that soluble Ym1 might
316 crystallize *in vivo* after i.t. injection. To test this, we stained BAL pellets using a polyclonal anti
317 Ym1/2 antibody and analyzed the samples using the ImageStream flow cytometry platform.
318 The results clearly showed that the i.t. injected pre-formed Ym1 crystals were still present as
319 intact crystals after 6 and 24 hours. The soluble Ym1 protein indeed crystallized *in vivo,* with
320 crystals being clearly detectable after 6 hours and accumulating further after 24 hours. The

321 crystals formed *in vivo* after i.t. injection of soluble Ym1 were also plate-like, but had a less
322 uniform distribution and were smaller in size than the i.t. injected Ym1 crystals (Fig. 2 F). The
323 total number of crystals found in the BAL pellet of soluble Ym1 treated mice (266 crystals in 5
324 pooled BAL pellets) was lower than in the BAL pellet of Ym1 crystal treated mice (1355 crystals
325 in 5 pooled BAL pellets), potentially explaining why the soluble Ym1 group had less
326 inflammation compared with the group receiving pre-formed Ym1 crystals.
327
328 **Ym1 crystals activate DCs in the lymph nodes.**
329 We next studied whether innate immunity triggered by Ym1 crystals was accompanied by the
330 induction of adaptive immunity, particularly since IL-1β, IL-33, IL-6 and TNFα in the lungs can
331 activate antigen presenting cells [41]. Airway DCs bridge innate and adaptive immunity and can
332 be activated by recombinant Gal10 crystals and monosodium urate (MSU) crystals [34,42].
333 Different subsets of DCs can be clearly distinguished from recruited monocytes and resident
334 macrophages based on the expression of CD26 and lack of expression of the complement C5a
335 receptor CD88, and further separated into $XCR1^+$ cDC1 and CD172 $(SIRP\alpha)^+$ cDC2 (see Fig. 3A
336 for gating strategy) [30,43]. In mice given Ym1 crystals in the presence of fluorescently-labeled
337 OVA antigen (Fig. 3 B), there was a clear increase in the number of total lung-draining mLN
338 $CD26^+CD88^-CD11c^+CD64^-$ conventional DCs (cDCs), numerically mainly caused by an increase
339 in the number of $CD172^+$ cDC2, compared with mice receiving PBS or soluble Ym1, although
340 $XCR1^+$ cDC1s also clearly reacted to the crystals. There was also an increase in the number of
341 mLN $CD88^+CD11b^+$ monocytes that expressed intermediate levels of CD11c induced by
342 crystals (Fig. 3 C). Not surprisingly, the exposure to crystalline Ym1 also led to an increase in
343 cDC1s, cDC2s and monocytes taking up the co-administered fluorescent OVA antigen (Fig. 3
344 D). Exposure to soluble Ym1 and Ym1 crystals also induced an upregulation of the
345 costimulatory molecules CD80 (data not shown) and CD86, and this effect was most
346 pronounced with crystalline Ym1, and particularly in cDCs that were also taking up fluorescent
347 OVA (Fig. 3 E).
348
349 **Ym1 crystals boost adaptive type 2 immunity.**
350 We next asked whether crystalline or soluble Ym1 could boost adaptive cellular immunity to
351 co-administered OVA, when DCs that have taken up antigen and matured migrate to mLNs
352 (Fig. 4 A). To evaluate induction of type 2 immunity in naïve antigen-specific T cells directly,
353 cell tracer violet labeled OVA-reactive $CD4^+$ T cell receptor (TCR) MHCII-restricted transgenic
354 T cells (OT-II T cells) crossed to the huCD2-IL-4 (KN2) reporter strain were transferred into WT
355 mice, allowing us to track T cell division simultaneously with the acquisition of a Th2-polarized
356 state *in vivo* [44]. When innocuous OVA was injected i.t. together with Ym1 crystals, the
357 adoptively transferred OT-II KN2 T cells showed increased proliferation 4 days (Fig. 4 B) and 7
358 days (data not shown) later in the mLNs, an effect absent when OVA was given with soluble
359 Ym1. This led to the accumulation of higher numbers of OT-II T cells and Th2 polarizing KN2+
360 OT-II T cells in the mLNs 4 days (Fig. 4 C) and 7 days (Fig. 4 D) after the i.t. administration. After
361 7 days, divided OT-II T cells and KN2+ OT-II T cells could also be found in the lungs of mice

362 receiving OVA mixed with Ym1 crystals (Fig. 4 E). These cells lost CD62L expression while
363 expressing CD44, showing they had become effector cells (data not shown). These effects on
364 T cell activation and Th2 polarization were again not observed when OVA was injected
365 together with soluble Ym1. Early IL-4 production in OVA-reactive OT-II cells could also point
366 to differentiation of T cells into T follicular helper (T_{FH}) cells that provide help for germinal
367 center reactions. However, we did not add CXCR5 or PD1 to study T_{FH} development in greater
368 detail.
369
370 We finally tested whether Ym1 crystals could also promote allergic type 2 inflammation to
371 inhaled harmless antigens, typically observed in asthmatics. WT C57BL/6 mice were sensitized
372 i.t. with OVA mixed with Ym1 crystals on days 0 and 1 and received OVA i.n. challenges on
373 days 11 to 13 (Fig. 5 A). These mice exhibited airway inflammation characterized by an influx
374 of eosinophils, B cells and T cells (Fig. 5 B), a higher production of the type 2 cytokines IL-5, IL-
375 10 and IL-13 in the supernatants of mLN restimulation cultures (Fig. 5 C) and a robust OVA-
376 specific IgG1 response, a hallmark of type 2 immunity, most likely driven by enhanced IL-4
377 production in Th2 or T_{FH} cells (Fig. 5 D). These effects were not observed when OVA alone was
378 used as the immunogen or when OVA was co-administered with soluble Ym1. Thus, the
379 induction of allergic type 2 inflammation was specifically related to the crystalline state of
380 Ym1. In contrast to recombinant Gal10 crystals, which mounted high titers of Gal10-specific
381 IgG1 antibodies when used as adjuvant in the same experimental set-up [34], Ym1 crystals did
382 not elicit an antibody response directed to Ym1 (Fig. 5 E). However, when mice received
383 repetitive injections of Ym1 crystals in a different set-up via i.p. injection (Fig. 5 F), high titers
384 of Ym1-specific IgM were detected (Fig. 5 G), suggesting that Ym1 crystals can trigger an auto-
385 immune response or elicit a recall response from natural IgM antibody producing peritoneal
386 B cells.
387
388 **Discussion**
389 Ym1 and Ym2 are among the most strongly induced proteins in the airways of mice after
390 allergen exposure[45-49] and both proteins readily form pseudo-CLCs *in vivo.* As a result, Ym1
391 and Ym2 have become markers of type 2 inflammation. Here we show by *ex vivo* X-ray
392 crystallography that Ym2 also crystallizes *in vivo* and that the phase transition of soluble
393 Ym1/Ym2 to crystalline pseudo-CLC states leads to profound immunostimulatory effects on
394 innate and adaptive type 2 immunity. Sutherland and colleagues have shown that vector-
395 based overexpression of Ym1 or Ym2 in the lung increased the number of neutrophils in the
396 BAL fluid [50]. Whether these observed effects were due to the crystalline or soluble state of
397 Ym1/2 remains unclear from these studies. Also in the present study, we lacked a proper
398 soluble Ym1 control, since ImageStream analysis showed the soluble Ym1 protein to readily
399 crystallize upon injection in the lungs. So far, several attempts to produce crystallization-
400 deficient soluble Ym1 or Ym2 muteins failed, despite the fact that this was feasible for the CLC
401 protein Gal10 [34]. In Persson *et al.* (2019), we produced anti-Gal10 antibodies able to dissolve
402 pre-existing CLCs and to inhibit key features of airway CLC crystallopathy in a humanized

403 mouse model of asthma [34]. Sutherland and colleagues have shown that blocking antibodies
404 directed against Ym1/2 suppressed neutrophilic inflammation in the lungs of asthmatic mice
405 and helminth-infected mice [34,50]. However, it is unclear if these anti-Ym1/2 antibodies used
406 suppressed lung neutrophilia by dissolving possible Ym1/2 pseudo-CLCs. We also observed
407 that Ym1 crystals induced an auto-antibody response of the IgM isotype, suggesting intrinsic
408 adjuvant activity in the crystalline state of Ym1. Antibodies to Ym1/2 have been described to
409 occur also in a model of incipient neoplasia in mice overexpressing the Epstein Barr virus
410 oncogene LMP1 in the skin, leading to chronic inflammation[51]. However, it is unclear if
411 induction of such auto-antibodies to Ym1/2 would be the result of spontaneous crystallization
412 of Ym1/2 in the skin of these mice. Recognition of endogenously produced MSU or cholesterol
413 crystals by IgM has been described previously [52,53], and in the case of MSU, it was even
414 proposed that IgM is required to turn soluble uric acid (UA) into an immunostimulatory
415 adjuvant [53]. Future studies will have to establish if IgM contributes in some way to the
416 adjuvanticity of Ym1 crystals or facilitates the transition of soluble to crystalline Ym1.
417 Ym1 (*Chil3*) and Ym2 (*Chil4*) share 95% nucleotide sequence identity and 91% amino acid
418 sequence identity and we now show here that native *in vivo* grown Ym1 crystals are
419 structurally similar to native *in vivo* grown Ym2 crystals. Given these similarities, we assume
420 that Ym2 crystals most likely will stimulate innate and adaptive immunity and act as a type 2
421 adjuvant, similar to Ym1 crystals, although we did not formally demonstrate this
422 experimentally. We can only speculate why, from an evolutionary perspective, mice even
423 express two very similar proteins that are expressed under similar conditions and share the
424 peculiar property to crystalize *in vivo*. However, Ym1 is mainly expressed by macrophages,
425 neutrophils and a subset of circulating pro-repair monocytes, while Ym2 is produced by lung
426 epithelial cells, which could have discrete context dependent benefits. We have also not
427 formally proven that Ym2 crystals have the same immunostimulatory effects on type 2
428 immunity as Ym1 crystals, but based on structural homology, we propose they do. Also, future
429 studies will have to elucidate if soluble Ym1 and Ym2 have similar effects on immunity and
430 tissue remodeling. A phase transition to its crystalline state may therefore mean different
431 things for Ym1 and Ym2 biology *in vivo*.
432 Understanding the requirements for protein crystal formation during type 2 immunity,
433 studying the mechanisms whereby protein crystals stimulate type 2 immunity and having the
434 proper tools to be able to distinguish between the soluble and the crystalline state will help
435 us to better understand if targeting CLCs in human asthma and chronic rhinosinusitis with
436 nasal polyps (CRSwNPs) would be of value. Since CLCs and pseudo-CLCs are almost exclusively
437 found in eosinophilic airway inflammation across many species, and share many biological
438 effects, it appears that protein crystallization is a more generalized feature of type 2 immunity.
439 The cellular influx and production of several cytokines and chemokines we observed after
440 recombinant Ym1 crystal injection was also observed in earlier work where recombinant
441 Gal10 crystals were injected into the lung of mice [34]. Besides triggering innate immunity, Gal10
442 crystals, just like Ym1 crystals were able to recruit and activate DCs, activate cellular and
443 humoral adaptive immune responses and act as type 2 adjuvants [34]. Besides, not only protein

444 crystals, but also organic non-proteinaceous crystals such as MSU crystals and crystalline alum
445 were able to recruit and activate DCs and act as type 2 adjuvants [42,54], suggesting that
446 promotion of type 2 response is a generic response to crystals of different chemical
447 composition. The convergent evolution of CLCs and pseudo-CLCs as protein crystals in type 2
448 immunity strongly suggests a selective evolutionary advantage of these protein crystals in the
449 enhancement of type 2-driven immune responses.
450

451 **Acknowledgements**

452 We acknowledge the crucial help of the staff of the VIB Protein Synthesis Core, the VIB Flow
453 Cytometry core, the VIB Bioimaging core, and. S.N.S., K.V., and K.H.G.V. thank the staff and
454 management of synchrotron beamlines P14 (PETRA 3, Hamburg, Germany), Proxima 1
455 (SOLEIL, Saclay, France), and PX1 (Swiss Light Source, Villigen, Switzerland) for beamtime
456 allocation and support during data collection of X-ray diffraction data.
457 B.N.L. acknowledges support from ERC advanced grant (789384 ASTHMA CRYSTAL CLEAR), a
458 concerted research initiative grant from Ghent University (GOA, 01G010C9), an FWO
459 Methusalem grant (01M01521) and an FWO EOS research grant (3G0H1222), and the Flanders
460 Institute of Biotechnology (VIB). S.N.S. acknowledges support to this project from the Ghent
461 University GOA program (BOF17-GOA-028).

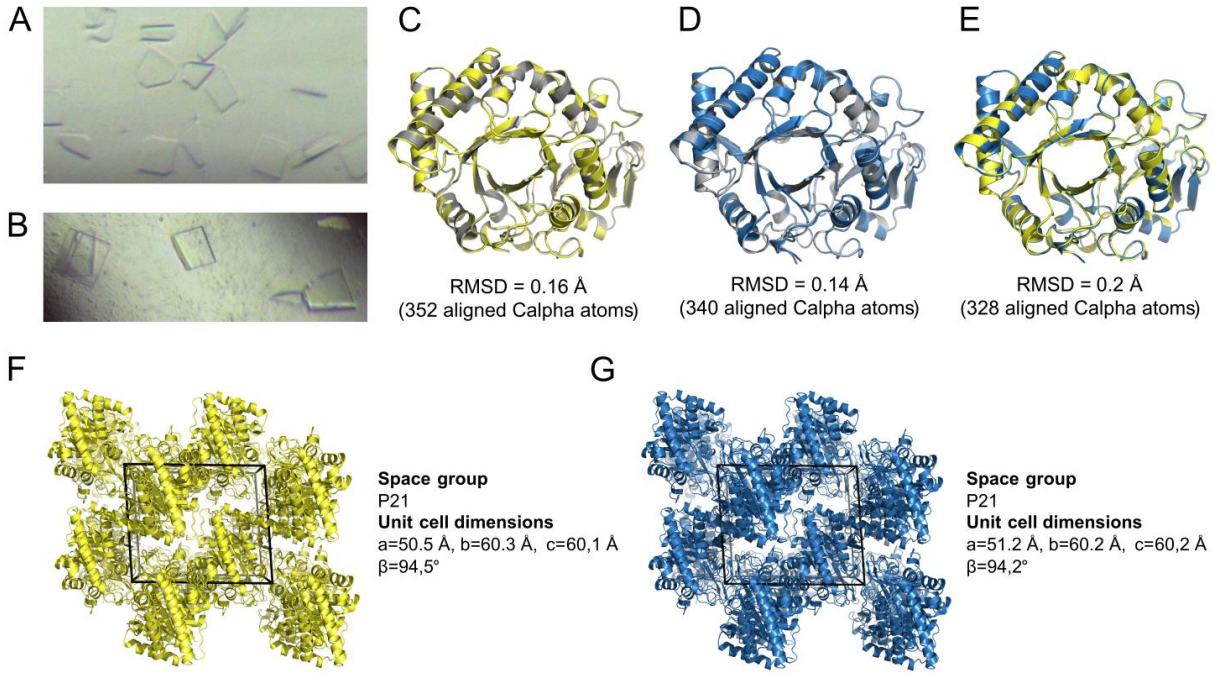

Figure 1: Recombinant Ym1 and Ym2 crystals are structurally similar to *in vivo* Ym1 and Ym2 crystals and to each other. A, B) Light microscopy pictures of recombinant Ym1 (A) and Ym2 (B) crystals. **C-E)** Structural superposition of the X-ray structures determined from a native *in vivo* grown Ym1 crystal isolated from the BAL fluid of me^{v}/me^{v} mice (C+E) (yellow), a native *in vivo* grown Ym2 crystal isolated from the BAL fluid of a C57BL/6J-Tg(CAG-Gal10)^{Bla} mouse (D+E) (blue) and a recombinant Ym1 (C) and Ym2 (D) crystal (grey). The low root-mean-square deviations (RMSDs) establish structural similarity. **F, G)** Crystal packing of *ex vivo* Ym1 (F) and Ym2 (G) crystals revealing their crystallographic equivalence.

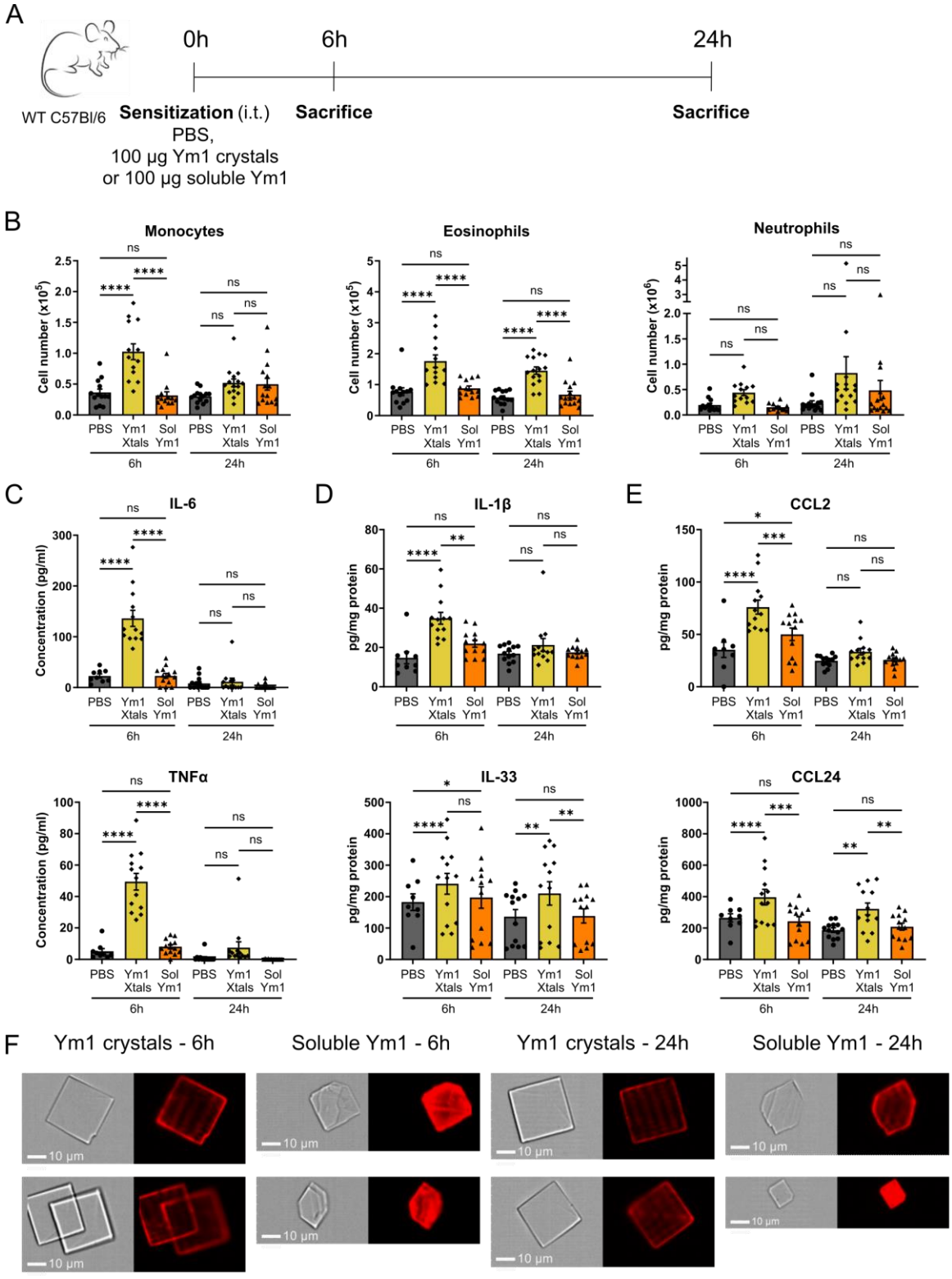
A
0h
6h
24h
WT C57Bl/6
Sensitization (i.t.)
PBS,
100 µg Ym1 crystals
or 100 µg soluble Ym1
Sacrifice
Sacrifice
B
Monocytes
Eosinophils
Neutrophils
Cell number (x10^5)
PBS
Ym1 Xtals
Sol Ym1
6h
24h
C
IL-6
D
IL-1β
E
CCL2
Concentration (pg/ml)
pg/mg protein
TNFα
IL-33
CCL24
F
Ym1 crystals - 6h
Soluble Ym1 - 6h
Ym1 crystals - 24h
Soluble Ym1 - 24h
10 µm

472

473 **Figure 2: Ym1 crystals activate innate immunity. A)** Scheme representing the innate immune response
474 experiment. **B)** Flow cytometric analysis of the immune cell influx in the lungs of PBS, Ym1 crystal and
475 soluble Ym1 treated mice measured 6 and 24 hours after i.t. injection. Data are pooled from 2 (for 6h
476 time point) or 3 (for 24h time point) independent experiments with n = 13, 13, 13, 14, 15 and 15,
477 respectively. **C)** Concentration of IL-6 and TNFα in the BAL fluid measured by ELISA. **D, E)** Concentration
478 of IL-1β, IL-33 (D), CCL2 and CCL24 (E) per milligram of protein of dispersed lung tissue measured by
479 ELISA. Data are pooled from 2 independent experiments with n = 13 per group. Data are shown as
480 mean ± SEM. ns P ≥ 0.05; *P < 0.05; **P<0,01; ***P <0.001; ****P < 0.0001. **F)** ImageStream pictures
481 of the BAL fluid of Ym1 crystal and soluble Ym1 treated mice 6 and 24 hours after i.t. injection. Samples
482 were stained with an antibody recognizing Ym1/2 (red).
483

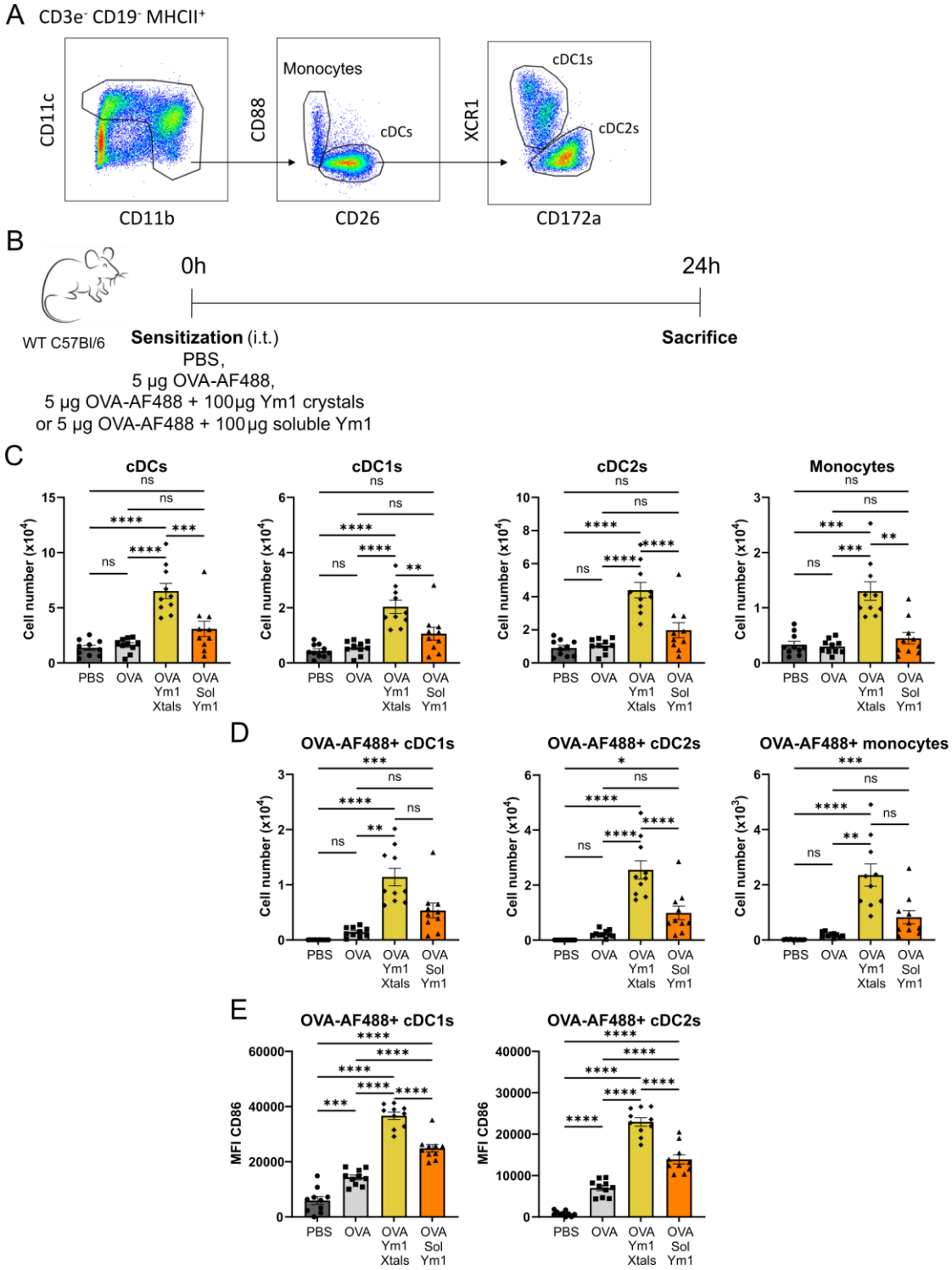

Figure 3: Ym1 crystals activate DCs in the lymph nodes. A) Gating strategy to distinguish different subsets of DCs and recruited monocytes. **B)** Scheme representing the DC activation experiment. **C, D)** Flow cytometric analysis of the DC and monocyte influx in the mLNs of PBS, OVA-AF488 alone, OVA-AF488 plus Ym1 crystals and OVA-AF488 plus soluble Ym1 treated mice measured 24 hours after i.t. injection. **E)** Median Fluorescence Intensity (MFI) of activation marker CD86 on OVA-AF488+ cDC1s and cDC2s of PBS, OVA-AF488 alone, OVA-AF488 plus Ym1 crystals and OVA-AF488 plus soluble Ym1 treated mice measured 24 hours after i.t. injection. Data are pooled from 2 independent experiments with n = 10 mice per group. Data are shown as mean ± SEM. ns $P \geq 0.05$; *$P < 0.05$; **P<0,01; ***P <0.001; ****$P < 0.0001$.

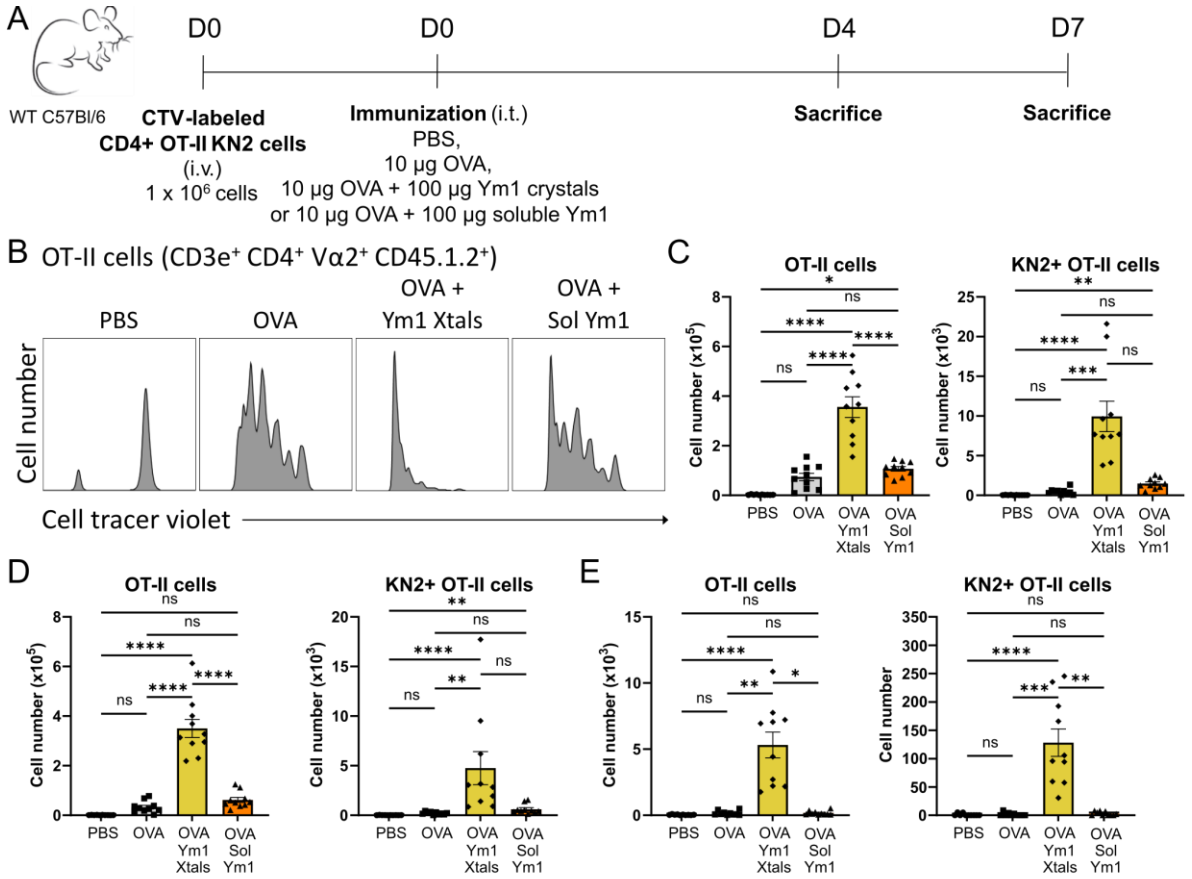

Figure 4: Ym1 crystals boost adaptive cellular immunity. A) Scheme representing the used adoptive transfer model. **B-E)** Proliferation and KN2 expression of OT-II T cells in the mLNs and lungs 4 and 7 days after i.t. administration of PBS, OVA alone, OVA plus Ym1 crystals or OVA plus soluble Ym1. (B) Representative histograms of the division profile of the adoptively transferred OT-II T cells ($CD3e^+$ $CD4^+$ $V\alpha2^+$ $CD45.1.2^+$) in the mLNs on day 4. (C, D) The numbers of OT-II T cells and KN2+ OT-II T cells in the mLNs on day 4 (C) and day 7 (D). (E) The numbers of OT-II T cells and KN2+ OT-II T cells in the lungs on day 7. Data are pooled from 2 independent experiments with n = 10 mice per group. Data are shown as mean ± SEM. ns $P \geq 0.05$; *$P < 0.05$; **P<0,01; ***P <0.001; ****$P < 0.0001$.

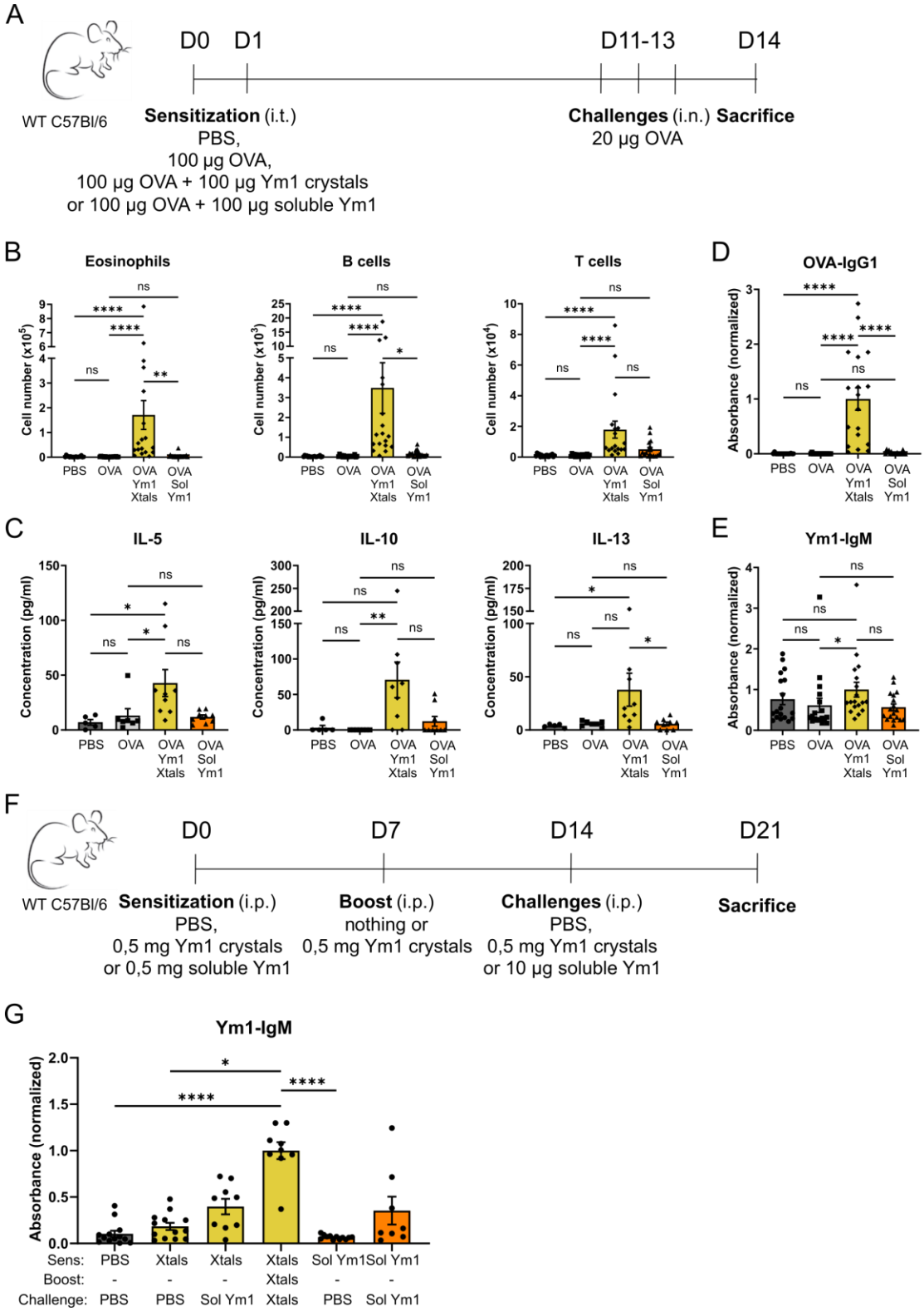

Figure 5: Ym1 crystals can act as type 2 adjuvant in OVA-induced asthma model and activate adaptive humoral immunity. A) Scheme representing the used OVA-induced asthma model. **B)** Flow cytometric analysis of the immune cell influx in the BAL fluid of mice sensitized i.t. with PBS, OVA alone, OVA plus Ym1 crystals or OVA plus soluble Ym1 and challenged i.n. with OVA. Data are pooled from 2 independent experiments with n = 18 per group. **C)** Levels of IL-5, IL-10 and IL-13 in the supernatant of mLN cells after restimulation with OVA for 20 hours. Data are from 1 experiment with n = 5, 7, 9 and 9, respectively. **D)** Serum OVA-specific IgG1 antibodies were measured by ELISA. **E)** Serum Ym1-specific

513 IgM antibodies were measured by ELISA. Data are pooled from 2 independent experiments with n =
514 18 per group. **F)** Scheme representing the adaptive humoral immune response experiment. **G)** Serum
515 Ym1-specific IgM antibodies were measured by ELISA. Data are pooled from 3 independent
516 experiments with n = 13, 13, 9, 9, 12 and 8, respectively. Data are shown as mean ± SEM. ns P ≥ 0.05;
517 *P < 0.05; **P<0,01; ****P < 0.0001. If pairwise comparison is not shown, the result is not significant.
518

References

1. Charcot, J. & Vulpian, A. Note sur des cristaux particuliers trouvés dans le sang et dans certains viscèresd'un sujet leucémique, et sur d'autres faits necroscopiques observés sur le même sujet. *Gaz. Hebd. de Méd et Chirurgie*, 755-758 (1860).
2. von Leyden, E. Zur Kenntniss des bronchial asthma. *(Virchov) Arch. Pathol. Anat.* **54**, 324-344. (1872).
3. Aegerter, H.*, et al.* Charcot-Leyden crystals and other protein crystals driving type 2 immunity and allergy. *Curr Opin Immunol* **72**, 72-78 (2021).
4. Doye, J.P., Louis, A.A. & Vendruscolo, M. Inhibition of protein crystallization by evolutionary negative design. *Phys Biol* **1**, P9-13 (2004).
5. Schönherr, R., Rudolph, J.M. & Redecke, L. Protein crystallization in living cells. *Biol Chem* **399**, 751-772 (2018).
6. Guo, L., Johnson, R.S. & Schuh, J.C. Biochemical characterization of endogenously formed eosinophilic crystals in the lungs of mice. *J Biol Chem* **275**, 8032-8037 (2000).
7. Hoenerhoff, M.J., Starost, M.F. & Ward, J.M. Eosinophilic crystalline pneumonia as a major cause of death in 129S4/SvJae mice. *Vet Pathol* **43**, 682-688 (2006).
8. Takamoto, M.*, et al.* Eosinophilia, parasite burden and lung damage in Toxocara canis infection in C57Bl/6 mice genetically deficient in IL-5. *Immunology* **90**, 511-517 (1997).
9. Shultz, L.D., Coman, D.R., Bailey, C.L., Beamer, W.G. & Sidman, C.L. "Viable motheaten," a new allele at the motheaten locus. I. Pathology. *Am J Pathol* **116**, 179-192 (1984).
10. Harbord, M.*, et al.* Ym1 is a neutrophil granule protein that crystallizes in p47phox-deficient mice. *J Biol Chem* **277**, 5468-5475 (2002).
11. Liu, Q.*, et al.* p47phox deficiency induces macrophage dysfunction resulting in progressive crystalline macrophage pneumonia. *Am J Pathol* **174**, 153-163 (2009).
12. Waern, I.*, et al.* Accumulation of Ym1 and formation of intracellular crystalline bodies in alveolar macrophages lacking heparanase. *Mol Immunol* **47**, 1467-1475 (2010).
13. Poczobutt, J.M.*, et al.* Altered Macrophage Function Associated with Crystalline Lung Inflammation in Acid Sphingomyelinase Deficiency. *Am J Respir Cell Mol Biol* **64**, 629-640 (2021).
14. Fallon, P.G., Emson, C.L., Smith, P. & McKenzie, A.N. IL-13 overexpression predisposes to anaphylaxis following antigen sensitization. *J. Immunol.* **166**, 2712-2716. (2001).
15. Rehm, S., Wcislo, A. & Deerberg, F. Non-neoplastic lesions of female virgin Han:NMRI mice, incidence and influence of food restriction throughout life span. II: Respiratory tract. *Lab Anim* **19**, 224-235 (1985).
16. Green, E. On the occurrence of crystalline material in the lungs of normal and cancerous Swiss mice. *Cancer Res* **2**, 210-217 (1942).
17. Murray, A.B. & Luz, A. Acidophilic macrophage pneumonia in laboratory mice. *Vet Pathol* **27**, 274-281 (1990).
18. Yang, Y.H. & Campbell, J.S. Crystalline excrements in bronchitis and cholecystitis of mice. *Am J Pathol* **45**, 337-345 (1964).
19. Feldmesser, M., Kress, Y. & Casadevall, A. Intracellular crystal formation as a mechanism of cytotoxicity in murine pulmonary Cryptococcus neoformans infection. *Infect Immun* **69**, 2723-2727 (2001).
20. Baldán, A., Gomes, A.V., Ping, P. & Edwards, P.A. Loss of ABCG1 results in chronic pulmonary inflammation. *J Immunol* **180**, 3560-3568 (2008).
21. Huffnagle, G.B., Boyd, M.B., Street, N.E. & Lipscomb, M.F. IL-5 is required for eosinophil recruitment, crystal deposition, and mononuclear cell recruitment during a pulmonary Cryptococcus neoformans infection in genetically susceptible mice (C57BL/6). *J. Immunol.* **160**, 2393-2400 (1998).
22. Mall, M.A.*, et al.* Development of chronic bronchitis and emphysema in beta-epithelial Na+ channel-overexpressing mice. *Am J Respir Crit Care Med* **177**, 730-742 (2008).

570 23. Roediger, B.*, et al.* IL-2 is a critical regulator of group 2 innate lymphoid cell function during
571 pulmonary inflammation. *J Allergy Clin Immunol* **136**, 1653-1663 e1657 (2015).
572 24. Henderson, W.R., Jr.*, et al.* A role for cysteinyl leukotrienes in airway remodeling in a mouse
573 asthma model. *Am J Respir Crit Care Med* **165**, 108-116 (2002).
574 25. Zhu, Z.*, et al.* Pulmonary expression of interleukin-13 causes inflammation, mucus
575 hypersecretion, subepithelial fibrosis, physiologic abnormalities, and eotaxin production. *J*
576 *Clin Invest* **103**, 779-788 (1999).
577 26. Leonidas, D.D.*, et al.* Crystal structure of human Charcot-Leyden crystal protein, an
578 eosinophil lysophospholipase, identifies it as a new member of the carbohydrate-binding
579 family of galectins. *Structure* **3**, 1379-1393 (1995).
580 27. Swaminathan, G.J., Leonidas, D.D., Savage, M.P., Ackerman, S.J. & Acharya, K.R. Selective
581 recognition of mannose by the human eosinophil Charcot-Leyden crystal protein (galectin-
582 10): a crystallographic study at 1.8 A resolution. *Biochemistry* **38**, 13837-13843 (1999).
583 28. Raes, G.*, et al.* Differential expression of FIZZ1 and Ym1 in alternatively versus classically
584 activated macrophages. *J Leukoc Biol* **71**, 597-602 (2002).
585 29. Ikeda, N.*, et al.* Emergence of immunoregulatory Ym1(+)Ly6C(hi) monocytes during recovery
586 phase of tissue injury. *Sci Immunol* **3**(2018).
587 30. Aegerter, H., Lambrecht, B.N. & Jakubzick, C.V. Biology of lung macrophages in health and
588 disease. *Immunity* **55**, 1564-1580 (2022).
589 31. Ward, J.M.*, et al.* Hyalinosis and Ym1/Ym2 gene expression in the stomach and respiratory
590 tract of 129S4/SvJae and wild-type and CYP1A2-null B6, 129 mice. *Am J Pathol* **158**, 323-332
591 (2001).
592 32. Parkinson, J.E., Pearson, S., Rückerl, D., Allen, J.E. & Sutherland, T.E. The magnitude of airway
593 remodeling is not altered by distinct allergic inflammatory responses in BALB/c versus
594 C57BL/6 mice but matrix composition differs. *Immunol Cell Biol* **99**, 640-655 (2021).
595 33. Van Dyken, S.J. & Locksley, R.M. Chitins and chitinase activity in airway diseases. *J Allergy Clin*
596 *Immunol* **142**, 364-369 (2018).
597 34. Persson, E.K.*, et al.* Protein crystallization promotes type 2 immunity and is reversible by
598 antibody treatment. *Science* **364**, 10.1126/science.aaw4295 (2019).
599 35. Kabsch, W. Integration, scaling, space-group assignment and post-refinement. *Acta*
600 *Crystallogr D Biol Crystallogr* **66**, 133-144 (2010).
601 36. Winn, M.D.*, et al.* Overview of the CCP4 suite and current developments. *Acta Crystallogr D*
602 *Biol Crystallogr* **67**, 235-242 (2011).
603 37. McCoy, A.J.*, et al.* Phaser crystallographic software. *J Appl Crystallogr* **40**, 658-674 (2007).
604 38. Emsley, P., Lohkamp, B., Scott, W.G. & Cowtan, K. Features and development of Coot. *Acta*
605 *Crystallographica Section D: Biological Crystallography* **66**, 486-501 (2010).
606 39. Bricogne G., B.E., Brandl M., Flensburg C., Keller P., Paciorek W., & Roversi P, S.A., Smart O.S.,
607 Vonrhein C., Womack T.O. . BUSTER version 2.10.3 *Cambridge, United Kingdom: Global*
608 *Phasing Ltd.* (2017).
609 40. Joosten, R.P., Long, F., Murshudov, G.N. & Perrakis, A. The PDB_REDO server for
610 macromolecular structure model optimization. *IUCrJ* **1**, 213-220 (2014).
611 41. Lambrecht, B.N. & Hammad, H. Lung dendritic cells in respiratory viral infection and asthma:
612 from protection to immunopathology. *Annu Rev Immunol* **30**, 243-270 (2012).
613 42. Kool, M.*, et al.* An unexpected role for uric acid as an inducer of T helper 2 cell immunity to
614 inhaled antigens and inflammatory mediator of allergic asthma. *Immunity* **34**, 527-540
615 (2011).
616 43. Rawat, K.*, et al.* CCL5-producing migratory dendritic cells guide CCR5+ monocytes into the
617 draining lymph nodes. *J Exp Med* **220**(2023).
618 44. Mohrs, M., Shinkai, K., Mohrs, K. & Locksley, R. Analysis of type 2 immunity in vivo with a
619 bicistronic reporter. *Immunity* **15**, 303-311 (2001).
620 45. Jeong, H.*, et al.* Proteomic analysis of differently expressed proteins in a mouse model for
621 allergic asthma. *J Korean Med Sci* **20**, 579-585 (2005).

46. Zhao, J., Zhu, H., Wong, C.H., Leung, K.Y. & Wong, W.S. Increased lungkine and chitinase levels in allergic airway inflammation: a proteomics approach. *Proteomics* **5**, 2799-2807 (2005).
47. Zhao, J., Yeong, L.H. & Wong, W.S. Dexamethasone alters bronchoalveolar lavage fluid proteome in a mouse asthma model. *Int Arch Allergy Immunol* **142**, 219-229 (2007).
48. Wong, W.S., Zhu, H. & Liao, W. Cysteinyl leukotriene receptor antagonist MK-571 alters bronchoalveolar lavage fluid proteome in a mouse asthma model. *Eur J Pharmacol* **575**, 134-141 (2007).
49. Wong, W.S. & Zhao, J. Proteome analysis of chronically inflamed lungs in a mouse chronic asthma model. *Int Arch Allergy Immunol* **147**, 179-189 (2008).
50. Sutherland, T.E.*, et al.* Chitinase-like proteins promote IL-17-mediated neutrophilia in a tradeoff between nematode killing and host damage. *Nat Immunol* **15**, 1116-1125 (2014).
51. Qureshi, A.M., Hannigan, A., Campbell, D., Nixon, C. & Wilson, J.B. Chitinase-like proteins are autoantigens in a model of inflammation-promoted incipient neoplasia. *Genes Cancer* **2**, 74-87 (2011).
52. Pilely, K.*, et al.* Cholesterol Crystals Activate the Lectin Complement Pathway via Ficolin-2 and Mannose-Binding Lectin: Implications for the Progression of Atherosclerosis. *J Immunol* **196**, 5064-5074 (2016).
53. Kanevets, U., Sharma, K., Dresser, K. & Shi, Y. A role of IgM antibodies in monosodium urate crystal formation and associated adjuvanticity. *J Immunol* **182**, 1912-1918 (2009).
54. Williams, G.R.*, et al.* Immunity induced by a broad class of inorganic crystalline materials is directly controlled by their chemistry. *J Exp Med* **211**, 1019-1025 (2014).

Table S1. Crystallographic data and refinement statistics[§,*]

Protein complex	Recombinant Ym1	*Ex vivo* Ym1	Recombinant Ym2	*Ex vivo* Ym2
Data collection				
X-ray source (beamline)	SOLEIL (Proxima 1)	PETRA III (P14)	PETRA III (P14)	SLS (PXI)
Wavelength (Å)	0.97857	0.9763	0.9763	1.0000089224
Space group	*P21*	*P21*	*P21*	*P21*
Cell dimensions				
a, *b*, *c* (Å)	50.33, 60.01, 60.12	50.52, 60.25, 60.12	51.09, 59.90, 59.88	51.26, 60.21, 60.17
α, β, γ (°)	90.00, 94.66, 90.00	90.00, 94.48, 90.00	90.00, 94.14, 90.00	90.00, 94.24, 90.00
Resolution (Å)	50.00-1.79 (1.90-1.79)	59.93-1.42 (1.50-1.42)	59.90-1.17 (1.24-1.17)	42.50-1.70 (1.81-1.70)
R_{meas} (%)	24.7 (112.1)	12.2 (138.2)	8.0 (35.8)	17.7 (136.4)
$< I/\sigma >$	5.28 (1.54)	8.99 (1.19)	15.12 (4.74)	6.59 (0.96)
CC ½ (%)	97.9 (56.6)	99.7 (39.5)	99.9 (92.5)	99.2 (35.8)
Completeness (%)	99.2 (96.0)	98.1 (97.3)	98.4 (95.9)	97.7 (97.3)
Redundancy	4.1 (3.9)	3.3 (3.3)	6.8 (6.1)	3.5 (3.4)
ISa score	8.04	26.18	27.31	24.20
Wilson B ($Å^2$)	20.318	20.936	12.048	24.584
Refinement				
Resolution (Å)	42.40-1.79	26.91-1.42	37.45-1.17	16.78-1.71
No. reflections	33 407	66 944	119 181	39 026
R_{work} / R_{free} (%)	17.29 / 19.86	18.10 / 20.52	15.75 / 16.73	17.71 / 20.48
No. non-H atoms				
Protein	2 957	2 957	2 976	2 970
Ligand/ion	10	4	24	6
Water	215	163	584	239
B-factors ($Å^2$)				
Protein	12.09	15.58	10.28	18.50
Ligand/ion	21.52	30.73	16.20	30.69
Water	21.74	22.78	27.02	27.93
R.m.s. deviations				
Bond lengths (Å)	0.008	0.010	0.010	0.010
Bond angles (°)	0.91	0.98	1.07	0.97

[§]Each dataset was collected from a single crystal. *Values in parentheses are for highest-resolution shell.